Geochimica et Cosmochimica Acta 413 (2026) 78–90

Contents lists available at ScienceDirect

Geochimica et Cosmochimica Acta

journal homepage: www.elsevier.com/locate/gca

Non-alkali metals titrate silica out of carbonatite melts into insoluble silicate minerals

Xinxiang Zhu [a], Michael Anenburg [b,*], Yan Liu [a]

[a] State Key Laboratory of Deep Earth and Mineral Exploration, Institute of Geology, Chinese Academy of Geological Sciences, Beijing 100037, People's Republic of China
[b] Research School of Earth Sciences, Australian National University, Canberra, ACT 2600, Australia

ARTICLE INFO

Associate editor: Olivier Namur

Keywords:
Silicocarbonatite
Antiskarn
Silica solubility
Carbonatite magma
Carbon cycle
Ferrocarbonatite

ABSTRACT

Silica solubility in crustal carbonatite melts is a controversial topic with suggested solubility limits varying wildly from nearly 0 % up to 15 % SiO_2. Here, we present experiments utilising alumina crucibles and CO_2 atmospheres. We tested low pressure phase relations and compositions in simplified Na–K–Ca–Fe^{3+}–Al–Si–F systems. We found that substantial mutual solubility of CaO and SiO_2 was not possible. Instead, they reacted to form combeite and other Na–Ca silicates. Kalsilite formed on crucible walls, and occasionally within the liquid pools. In Fe_2O_3-rich systems, SiO_2 was likewise poorly soluble in the carbonatite melt with both components partitioning to separate silicate phases. Silica is substantially soluble in carbonatite melts only if they contain Na_2O or K_2O and no other non-alkali cations that can react with SiO_2 to form refractory silicates. In these alkali-dominated systems, immiscible silicate liquids form in equilibrium with Si-bearing, Ca-poor carbonatite melts. Our findings agree with experimentally-derived carbonatite compositions obtained over the past several decades, particularly in decreasing temperatures and increasing alkali regimes. The Ca-poor character of both experimental immiscible liquids may explain the unusual alkali-rich composition of carbonatites and nephelinites in Oldoinyo Lengai, formed at near-atmospheric pressures. Since virtually all natural carbonatite melts contain much more Ca (and other non-alkali metals such as Mg or Fe) than Si, actual natural melt compositions will be SiO_2-free for all practical purposes at temperatures below approximately 1000 °C, resulting from SiO_2 being titrated out to refractory silicates. We propose that low-temperature silicocarbonatites are likely to be antiskarns, igneous silicate mineral assemblages within carbonatites where SiO_2 was externally supplied by adjacent silicate rocks. Likewise, we suggest that many carbonatite-associated silicate rocks in ring complexes did not entirely form as cumulates from SiO_2-bearing carbonatite melts. Instead, some formation by antiskarn metasomatism is a plausible mechanism. We suggest that currently-observed quartz in carbonatites forms post-magmatically. Therefore, previously hypothesised silica-dependent ore-forming processes may not occur in natural carbonatites, because SiO_2 cannot attain sufficient concentrations in primary carbonatitic melts and mineralising fluids.

1. Introduction

Carbonatites, rocks composed primarily of calcite and dolomite, crystallise out of carbonatite melts (Yaxley et al., 2022). These rocks are typically understood as cumulates that do not faithfully record the composition of the melts from which they formed (Guzmics et al., 2011; Mitchell, 2005; Schmidt et al., 2024). Only one carbonatite melt has been observed in nature: the natrocarbonatite lava of Oldoinyo Lengai (Dawson, 1962), and there are debates on how typical this lava is compared to the overall range of melt compositions that lead to carbonatite rock formation (Chayka et al., 2021; Guzmics et al., 2011; Weidendorfer et al., 2017). The uniqueness of Oldoinyo Lengai means that the compositional range of presumably typical carbonatite melts remains enigmatic and has never been measured. Instead, melt compositions are inferred by indirect methods, including melt inclusion studies (Berkesi et al., 2020; Guzmics et al., 2019; Kamenetsky et al., 2021; Veksler and Lentz, 2006) and experimental petrology (Anenburg and Aslam, 2024; Brooker and Kjarsgaard, 2011; Chebotarev et al., 2019; Lee and Wyllie, 1998b, 2000; Yang et al., 2024).

One of the major contention points regarding magmatic compositions is the permissible levels of silica contents in carbonatite melts. Experimental studies show that at crustal pressures and below about

* Corresponding author.
E-mail addresses: zxxcags@126.com (X. Zhu), michael.anenburg@anu.edu.au (M. Anenburg), ly@cags.ac.cn (Y. Liu).

https://doi.org/10.1016/j.gca.2025.10.037
Received 21 May 2025; Accepted 28 October 2025
Available online 1 November 2025

1000 °C, silica contents of alkali carbonatite melts are typically under 2 %—and often lower than 1 %—when saturated with silicate minerals or an immiscible silicate melt (Anenburg and Aslam, 2024; Brooker and Kjarsgaard, 2011; Guo et al., 2024; Martin et al., 2013; Xue et al., 2024). Higher silica contents are only possible in alkali-poor carbonatite melts (i.e., with $Na_2O + K_2O$ lower than around 10 %), but even then, SiO_2 content is almost always below 10 % if temperature is lower than about 1000 °C (Brooker and Kjarsgaard, 2011; Nabyl et al., 2020; Otto and Wyllie, 1993; Wyllie and Haas, 1965).

Despite the supposed low silica solubility, silicate minerals are rather common in carbonatites, with some rocks reaching sufficient silicate abundance to be termed silicocarbonatites, defined by Le Maitre et al. (2002) as containing at least 20 % SiO_2 (see further discussion in Mitchell, 2005; Mitchell and Gittins, 2022; Yaxley et al., 2022). Does this SiO_2 content in the rock reflect an equivalent amount of dissolved SiO_2 in the melt? To this end, characteristic silicate minerals (e.g., phlogopite or olivine) that contain 40 % SiO_2 at a modal proportion of 50 % will produce a silicocarbonatite. Silicocarbonatite-hosted silicates often appear magmatic, but paradoxically this would require unrealistically high SiO_2 content of ~20 % in the melt, around one order of magnitude higher than observed in the above-mentioned experimental work. This problem is exacerbated when minerals with higher SiO_2 contents, such as clinopyroxenes or amphiboles, are present.

Despite abundant experimental data, low SiO_2 contents in sub-1000 °C carbonatite melts are not universally accepted. Lee and Wyllie (1994) reported 15 % SiO_2 in an experimental Ca–Na-rich carbonatite melt quenched from 833 °C, serving as one of the earliest applications of microanalytical methods to carbonatite systems. Similarly, a recent melt inclusion study suggested that some moderately alkaline carbonatite melts can dissolve around 15 % silica (Berndt and Klemme, 2022), which sparked some debate (Anenburg and Guzmics, 2023; Berndt and Klemme, 2023). Furthermore, Yuan et al. (2024) experimentally crystallised quartz and various other silicates out of an artificially SiO_2-rich brine-melt (a highly alkaline and evolved carbonatite melt, see Yaxley et al., 2022) across a temperature range of about 700 °C to 500 °C, indicating appreciable SiO_2 contents in their experimental carbonatite melts. Evidently, some discrepancies exist between the various experimental and natural rock studies, necessitating further study.

The range of permissible silica contents in carbonatite melts is of utmost importance, as carbonatite rocks often contain silicate minerals. Whether these silicate minerals originate from endogenous or external silica provides insights into the metasomatic capacity of carbonatite melts. Watkinson and Wyllie (1971) suggested that carbonated silicate liquids can form calcite following silicate mineral fractionation, explaining igneous alkaline–carbonatite complexes as magmatic differentiation products of carbonated silicate liquids. Lee and Wyllie (1998a) demonstrated that carbonate-bearing and MgO-poor magmas may fractionate sufficient silicate materials for calcite to join the liquidus. This causes precipitation of a magmatic calcite–silicate mineral assemblage, implying a SiO_2-rich carbonatite melt. Consequently, that carbonatites and their associated silicate rocks form as late differentiates of a single magma was occasionally adopted to explain several natural occurrences (Ackerman et al., 2021; Doroshkevich et al., 2017; Savard and Mitchell, 2021). Nevertheless, Kjarsgaard (1998) observed that such magmas are too Si-rich to be considered carbonatitic, as they only contain a small carbonate component. Instead, these calcite-precipitating silicate liquids resemble conjugate phases to true carbonatite melts, which are naturally more important to carbonatite rock formation. Finally, these differentiation models typically invoke melilite or nepheline fractionation (Kjarsgaard, 1998; Watkinson and Wyllie, 1971), which cannot explain the broader silicate mineral diversity observed in silicocarbonatites and other silicate-bearing carbonatites.

Recently developed alternative models for silicate formation within carbonatites propose that silica-free carbonatite melts react with their silicate host rocks, forming silicate mineral assemblages termed antiskarns (Anenburg and Mavrogenes, 2018; Chmyz et al., 2022; Giebel et al., 2019). These carbonatite–silicate reactions may explain the common observation of ultramafic rings within and around carbonatite complexes (Anenburg and Walters, 2024; Vasyukova and Williams-Jones, 2022). Silica content in carbonatites strongly influences rare earth element (REE) and niobium mineralisation style in carbonatites (Vasyukova and Williams-Jones, 2023; Voropaeva et al., 2024; Williams-Jones et al., 2024; Zheng et al., 2023). Thermodynamics constrains that silica and carbonate are often mutually exclusive in carbonatite melts, with introduction of silica causing degassing of carbonate as CO_2 (Anenburg and Walters, 2024; Massuyeau et al., 2015; Mororó et al., 2024). Thus, the degree of silica solubility in carbonatites can control short-term spikes of atmospheric carbon dioxide emissions from carbonatite systems, with measurable climate effects (Gales et al., 2020; Paulsen et al., 2017).

Most experimental work to date has focused on compositional determination of immiscible carbonatite and silicate melts at equilibrium (Brooker and Kjarsgaard, 2011; Kjarsgaard, 1998; Martin et al., 2013; Nabyl et al., 2020; Weidendorfer and Asimow, 2022). Additional experimental studies investigated processes leading to carbonatite-associated ore formation (Anenburg et al., 2020b; Williams-Jones et al., 2024; Yuan et al., 2024). Some studies reported silica contents in carbonatites as a secondary outcome of experiments characterising element partitioning (Guo et al., 2024; Nabyl et al., 2021; Xue et al., 2024). However, no study specifically investigated silica solubility in crustal conditions as a function of carbonatite melt composition.

We suggest that the surprisingly high silica solubility observed by Yuan et al. (2024) resulted from their experimental starting materials, which included quartz crystals. This silica reacted to form various insoluble silicates such as aegirine, cancrinite, and britholite, as expected in antiskarn-type reactions. Other experimental studies formed wollastonite (Anenburg and Aslam, 2024; Anenburg and Mavrogenes, 2018; Vasyukova et al., 2023), phlogopite (Williams-Jones et al., 2024), and various other mafic minerals such as clinopyroxenes and amphiboles (Anenburg and Mavrogenes, 2018; Vasyukova et al., 2023). All these minerals share a key commonality: they contain the non-alkali metals Ca, Mg, or Fe. Alumina is also important, with alkali feldspars or feldspathoids often stable in presumed carbonatite–silicate reaction zones (Anenburg and Walters, 2024). This leads to a possible explanation for quartz crystallising out of the Yuan et al. (2024) carbonatitic brine-melts: they had more silica than required to sequester all non-alkali metals. Pure alkali silicates such as ertixiite ($Na_2Si_4O_9$) and natrosilite ($Na_2Si_2O_5$) were never reported in experimental studies of carbonatites, and are similarly not found in natural carbonatites. This indicates they are not stable in carbonatite systems, and once non-alkali metals and alumina are consumed by reaction to refractory silicates, the fate of any remaining silica is one of two: (1) dissolve in Na–K carbonatite melt, or (2) form quartz. We hypothesise that Yuan et al. (2024) demonstrated both, with silica dissolving into the melt at higher temperatures and crystallising to quartz during cooling.

Here, we perform experiments to address this knowledge gap and directly explore the relationship between alkali carbonatite melts, silica, and non-alkali metals. We then quantify silica solubility across varying Ca/Si ratios by measuring SiO_2 content of the carbonatite melt at silicate phase saturation, including silicate liquid or silicate minerals.

2. Methods

2.1. Experimental

We conducted 14 experiments using bulk starting compositions as given in Table 1. Our experiments were conducted in 1 atm gas mixing furnaces using open alumina crucibles in pure CO_2 atmospheres (Fig. 1a). These furnaces are designed to idle at 600 °C, and insertion of the loaded crucibles causes a sudden temperature increase. This leads to rapid melting and gas expansion, forming bubbles that pop and spray the experimental charge such that it is lost to the bottom of the furnace. In

Table 1
Run conditions, bulk starting compositions, and experimental products for 1 atmosphere experiments. Abbreviations: CM–carbonatite melt; SM–silicate melt, FM–iron-rich silicate melt; Kls–kalsilite, Cbe–combeite; NCSP–calcic sodium silicate perovskite; NCSC–cubic calcic sodium silicate.

Run name	Temperature (°C)	Duration (h)	Cooling rate (°C/min)	Na_2CO_3 (wt%)	K_2CO_3 (wt%)	$CaCO_3$ (wt%)	CaF_2 (wt%)	SiO_2 (wt%)	Fe_2O_3 (wt%)	Product phases
NKS	850	26		44.5	47.5			8.0		CM, Kls
NKS16	850	170		40.6	43.4			16.0		CM, SM1, SM2, Kls
7NKS16	850 to 750	176	2	40.6	43.4			16.0		CM, SM, NMS, Kls
9NKS16	950	97		40.6	43.4			16.0		CM, SM, Kls
NKCS	850	26		37.8	40.4	13.8		8.0		CM, Kls, NCSP
NKCS8	850	170		37.8	40.4	13.8		8.0		CM, Kls, NCSP, Cbe
7NKCS8	850 to 750	176	2	37.8	40.4	13.8		8.0		CM, Kls, Cbe
9NKCS8	950	97		37.8	40.4	13.8		8.0		CM, Kls, NCSP
NKFS*	850	170		39.3	41.9	0.0	10.8	8.0		CM, Kls, Cbe
NKCFS*	850	170		38.3	40.9	9.2	3.6	8.0		CM, Kls, NCSP, Cbe
NKCFS1*	850	170		38.8	41.4	4.6	7.2	8.0		CM, Kls, NCSP, Cbe
NKCS516	850	170		38.6	41.2	5.0		15.2		CM, SM, Kls, NCSC
NKFeS1	850	170		37.8	40.4			8.0	13.8	CM, SM, FM, Kls
NKFeS2	850 to 600	116	0.1	37.8	40.4			8.0	13.8	CM, SM, FM, Kls

*CaF_2 amounts calculated to replace $CaCO_3$ on a mole-by-mole basis.

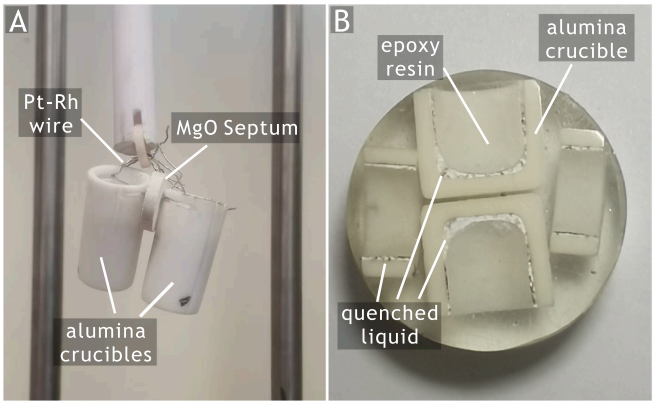

Fig. 1. (a) Filled alumina crucible setup prior to experiment commencement. (b) Both sections of a single experiment (run NKCFS) mounted in a one-inch epoxy mount, showing excellent wetting of the carbonatite liquid on the alumina crucible such that substantial ponding at the bottom is almost non-existent. The crucible tops were also cut and placed in the same mount in order to provide uniform hardness throughout the mount during polishing.

order to mitigate sample loss, we took several steps to decrease the volume and porosity of the starting mix. First, we mixed the two primary components, Na_2CO_3 and K_2CO_3, in a nearly-eutectic 55:45 molar mixture, respectively. This mixture was briefly melted in a nickel crucible above the eutectic point of 710 °C. The liquid was poured into a graphite dish for rapid solidification, resulting in predominantly single phase $(Na,K)_2CO_3$. This mixture was then combined with the other starting materials by grinding in acetone using an agate mortar and pestle, as shown in Table 1.

Alumina crucibles of > 99 % purity, with micrometre-scale grains of MgO, SiO_2 and ZrO_2 comprising the remaining < 1 % as common contaminants, were pre-drilled in their tops such that they can be hung on metal wires (Fig. 1a). Then, each experimental charge was inserted into the crucible and packed as tightly as possible. Once the crucibles were filled to about a third of their height, they were gradually heated in a box furnace up to 550 °C in steps of 50 °C for 15 to 30 min per step. At around 400 °C, sintering and some volume loss were observed, and the charge was crushed inside the crucible and tightly packed again. At around 550 °C, substantial volume loss was observed due to sintering and potential small-scale eutectic melting. This denser charge was again recompacted inside the crucible.

Up to three crucibles were used in a single experiment, joined and suspended from a vertical alumina rod using Pt–Rh alloy wires repurposed from scrap type B thermocouples (Fig. 1a). When two or three experiments were run, they were separated by an MgO septum to ensure that no cross-contamination occurred as gas bubbles inevitably pop (Fig. 1a). The alumina rods were lowered through the top furnace hatch. Heating from 600 °C to target temperatures (Table 1) progressed at 2 °C·min^{-1}. Experiments with a target temperature of 750 °C were initially heated to 850 °C, dwelled for 5 h and then cooled to 750 °C at 2 °C·min^{-1} for final dwell. One ferric experiment was heated to 850 °C, dwelled for 48 h, then cooled to 600 °C at 0.1 °C·min^{-1} for final dwell. All experiments were run in a gas flow of pure CO_2 at a rate of 100 mL per minute. Evaporation rate of volatile species (e.g., the alkalis) at these conditions is estimated as negligible, and in any case much slower than rapid equilibration within the carbonatite melt. As long as final compositions can be successfully measured, syn-experiment modifications to the semi-arbitrary starting compositions were inconsequential. Pure CO_2 atmospheres at our conditions typically result in oxygen fugacity approximately 2 log units above the magnetite–hematite buffer. The CO_2 atmosphere ensures that the calcic carbonate component in the melt does not thermally decompose, and any reactions are solely due to SiO_2 incorporation (for a detailed discussion on this method, see Anenburg and Aslam, 2024). Due to the resulting liquids having low viscosities, the experiments were not quenched by dropping them below the bottom of the furnace as this would cause spraying and material loss. Instead, the experiments were gently raised through the hatch and within three to four seconds, their bottoms were immediately dipped in water, taking care that no water leaked into the water-soluble material inside. Quenching to the solid state occurred in roughly two seconds, evident by the hissing sound duration marking the transition across the boiling point of water (100 °C). Whilst this led to a cooling rate slower than traditional quenching methods (such as dropping to water directly from the furnace), no material was lost, and cooling was sufficiently rapid to mostly preserve compositions and textures of the various experimental phases.

Once the crucibles were cool enough to touch after several tens of seconds, they were mounted and covered by epoxy resin to isolate the experimental products from atmospheric moisture. After initial hardening, each crucible was rapidly sliced in half using a water-cooled rock saw to expose a vertical section. This water exposure was sufficiently brief to prevent significant carbonate dissolution, such that any affected surface layer can be easily polished away. The halves were immediately wiped, placed in a 120 °C oven for drying, and then remounted in epoxy resin (Fig. 1b). The mounts were protected by epoxy and placed inside a small chamber filled with desiccating cobalt-based silica beads.

2.2. Analytical

Shortly before analysis, the samples were dry-polished using SiC paper to remove about 200 μm of surface material containing atmospheric-reacted and water-damaged layers, to expose unaltered

material that did not encounter water. This was followed by diamond polishing using oil lubrication in grit size steps of 3 μm, 1 μm, and ¼ μm. The samples were cleaned with petroleum spirit in an ultrasonic bath to remove the oil, carbon coated, and immediately taken to scanning electron microscope (SEM) observation using a Hitachi 4300 SE/N field emission instrument. The samples were kept inside the desiccator-filled chamber during transport between these steps and instruments. Microbeam analysis using wavelength dispersive spectroscopy (WDS) was unsuitable for our experimental products, as it can only measure five elements simultaneously at best. It requires relatively high beam currents, destroying the beam-sensitive alkali-rich carbonates before additional elements could be measured. Whilst the analytical beam can be defocused, this introduces a detrimental matrix effect. Instead, compositions were obtained by energy dispersive spectroscopy (EDS) with an Oxford Instruments INCA X-MAX 80 mm^2 silicon drift detector system (SDD; demonstrated to produce data of equivalent quality to WDS, Çubukçu et al., 2008; Ritchie et al., 2012; Ross and Simon, 2019). The EDS system is calibrated with reference materials providing non-normalised analytical totals, allowing CO_2 content estimation. Calibration was performed on an Astimex block using albite, periclase, diopside, sanidine, tugtupite, and pyrite. Analytical conditions were an accelerating voltage of 15 kV and a beam current of 600 pA. Even at these modest beam settings, alkalis were highly volatile. Small phases in which only point analyses were possible were measured for 30 s, silicate glasses and crystalline silicate grains were measured for 60 s, and carbonatite liquids were measured for 180 to 240 s. Despite the focused beam used in our SEM, dwell times per point during raster mode were typically on the millisecond range, minimising beam damage to alkali-rich materials. Where possible, large areas—on the order of tens of square micrometres—were measured to average heterogeneous quench materials and avoid alkali migration under the electron beam (Fig. 2).

3. Experimental descriptions and results

Our carbonatite melt compositions were measured by rastering an electron beam over a large area during EDS analysis (Fig. 2). These areas often include porosity, epoxy resin, and various foreign materials captured in small cracks during polishing, leading to a large scatter in analytical totals. Despite efforts to minimise contact with atmospheric moisture, minor efflorescence occurred on some samples (e.g., Fig. 3a). To bring all analytical results to an equal footing, we calculated the CO_2 content that should be present based on Na_2O, K_2O, and CaO. We excluded SiO_2 and Al_2O_3 from the carbonate-bound elements as empirical evidence from previous experimental studies shows that analytical totals of quenched carbonatite melts tend to increase almost linearly with increasing SiO_2 and Al_2O_3 (Brooker and Kjarsgaard, 2011; Martin et al., 2013; Weidendorfer and Asimow, 2022). This indicates that Si and Al do not have a stoichiometric associated carbonate counterpart in the melt structure. Finally, we derived a new total, which was subsequently normalised to 100 % along with all measured components (Table 2).

3.1. Na–K–Si

Experiments NKS, NKS16, 7NKS16, and 9NKS16 all resulted in abundant carbonatite melt solidified into various dendritic and feathery textures, as is typical of quenched carbonatite melts (Fig. 3b). This indicates that the water-damaged layer was successfully removed, exposing fresh material that faithfully represents the quenched carbonatite melt. Many individual feathers were exceptionally long, reaching lengths of several millimetres. Due to the somewhat slow quenching rate, minor fractionation occurred with some areas showing a brighter BSE contrast, mostly deriving from a higher K_2O/Na_2O ratio (Fig. 3c). All three 16 % SiO_2 experiments had coarse immiscible silicate glasses coexisting with the carbonatite melt (Fig. 3b). Experiment NKS contains rare bubble-like silicate glasses up to 20 μm across (Fig. 3d). While appearing as immiscible silicate liquids, they probably formed on quench because they are often truncated by the more abundant carbonates. This indicates that experiment NKS was not saturated with an immiscible silicate liquid. Experiment NKS16 contains a large silicate zone in the bottom (Fig. 3b). It is separated into an upper layer (bright in BSE contrast) and a lower layer (dark in BSE contrast). Both layers were highly beam sensitive, resulted in low analytical totals (Table 3), and contained round carbonatite melt bubbles. Therefore, each layer had properties consistent with being a quenched liquid on its own, but the reason for the existence of two layers is uncertain. We suspect one of three reasons: (1) high temperature equilibrium immiscibility between two silicate liquids, (2) separation during quench, or (3) a solidification front of an amorphous alkali silicate through the liquid as the experiment progressed.

Kalsilite occurred in all experiments as a coating on the interior of the alumina crucible, in contact with quenched carbonatite melt and occasionally with silicate glass, when present. In 7NKS16, several skeletal kalsilite crystals probably formed during the cooling stage from 850 °C to 750 °C (Fig. 3e). In 9NKS16, rare needle-shaped kalsilite was found within the carbonatite, in addition to the crucible wall (Fig. 3f). Thermal contraction and cracking are evident, particularly in the internal contacts between experimental charges and alumina crucibles. These cracks

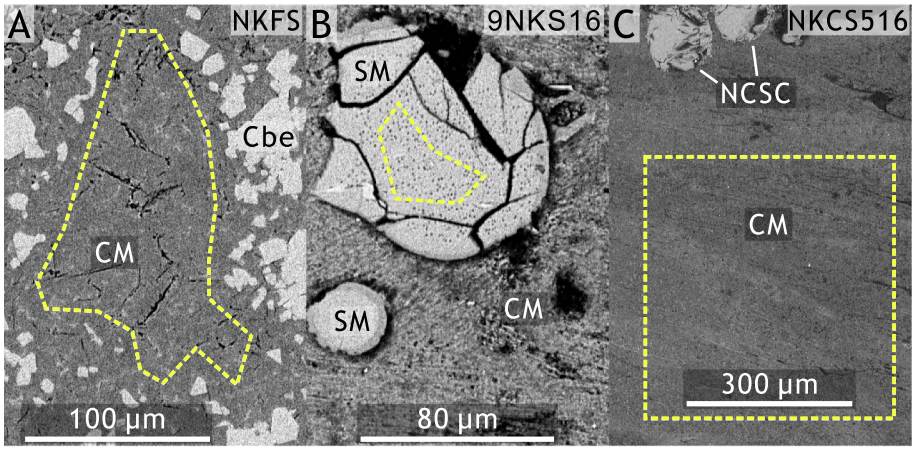

Fig. 2. Backscattered electron images showing examples of rastered areas for compositional analysis marked with yellow dashed lines, showing (A) interstitial quenched carbonatite melt between combeite crystals, (B) silicate glass, and (C) large areas of clean quenched carbonatite melt. Sample names given in top right corner of each panel. Abbreviations as in Table 1.

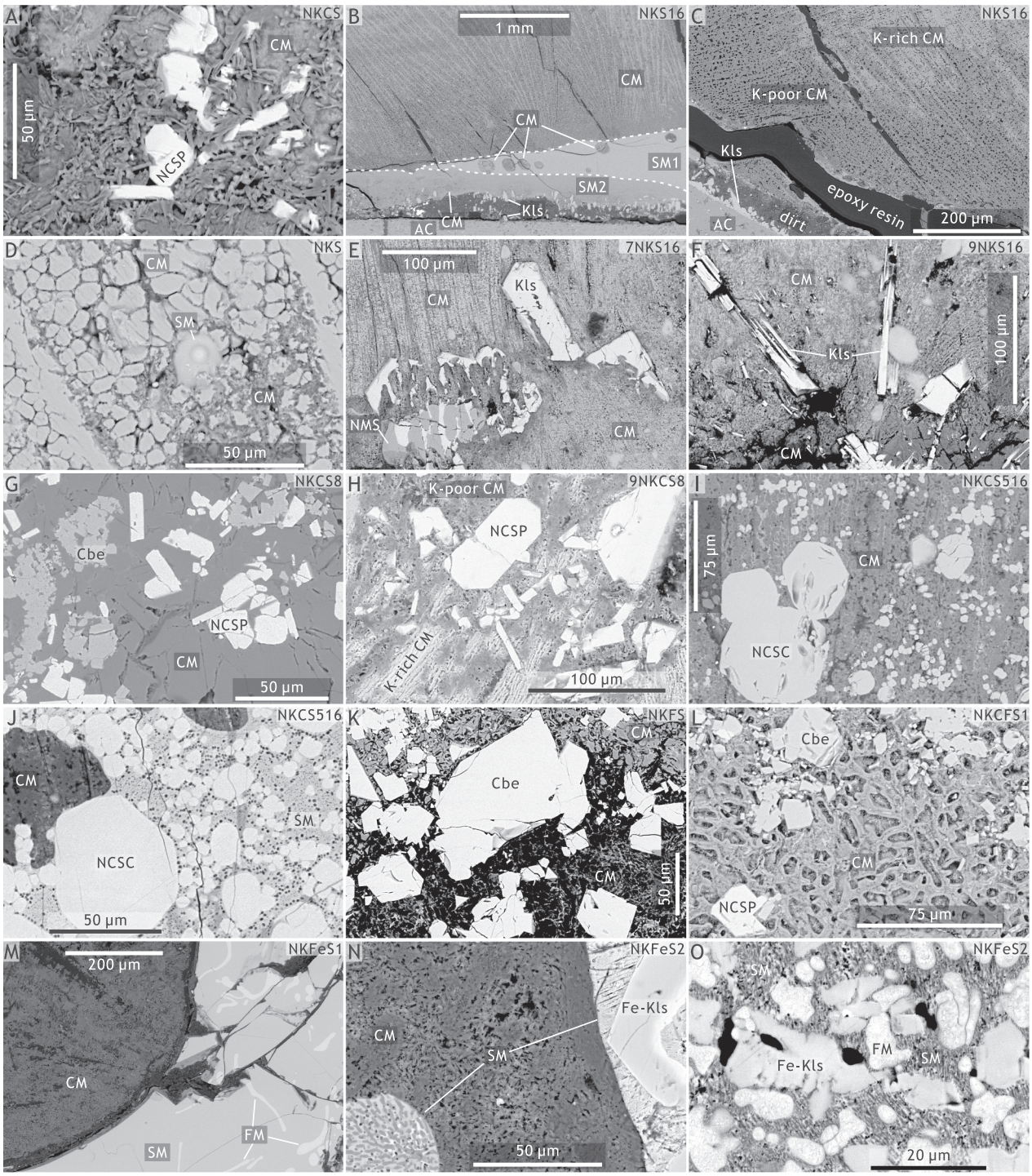

Fig. 3. Backscattered electron images of experimental products. (A) NKCS: NCSP crystals in carbonatite melt matrix. Some alkali efflorescence, most likely NaOH or Na_2CO_3, covers the polished surface. (B) NKS16, from top to bottom: Quench carbonatite dendrites, glassy silicate phases with bubbles of quenched carbonatite melt, kalsilite, cutting dirt, and alumina. (C) NKS16: Differentiation of the quench carbonatite to K-rich and K-poor dendrites. Also shown is kalsilite in contact with the alumina crucible. Cutting dirt and epoxy resin filling thermal cracks and large fracture formed during cutting, respectively. (D) NKS: Quenched carbonatite melt showing small silicate globule that probably exsolved upon cooling. The internal ring with variable brightness resulted from electron beam damage during EDS spot analysis. (E) 7NKS16: Skeletal kalsilite, sodium metasilicate, and quenched carbonatite dendrites. (F) 9NKS16: Acicular kalsilite in a matrix of quenched carbonatite melt. K-rich efflorescence appears as dull light grey patches. (G) NKCS8: Non-dendritic quenched carbonatite melt with phenocrysts of NCSP and combeite. (H) 9NKCS8: Quench carbonatite melt differentiated to K-rich and K-poor domains with euhedral crystals of NCSP. (I) NKCS516: NCSC with a seriate size distribution in a matrix of quenched carbonatite melt. (J) NKCS516: Immiscible carbonatite and silicate melts. NCSC is preferentially wet by the silicate phase. (K) NKFS: Euhedral combeite crystals in quenched carbonatite melt. Polishing difficulties lead to a poorly-imaged surface in the bottom part of the image. (L) NKCFS1: Coexisting NCSP and combeite in a matrix of vermicularly-quenched carbonatite melt. (M) NKFeS1: Three-way immiscibility between carbonatite, silicate, and Fe-rich silicate melts. (N) NKFeS2: Immiscible quenched carbonatite and silicate melts. Fe-rich kalsilite is found within the silicate melt. Zoning indicates higher Fe and lower Al towards the rims. (O) NKFeS2: Three-way immiscibility between carbonatite, silicate, and Fe-rich silicate melts, with Fe-rich kalsilite phenocrysts. Abbreviations as in Table 1.

Table 2
Normalised compositions of quenched carbonatite melts.

Run name	Na_2O	MgO[a]	Al_2O_3	SiO_2	SO_3[b]	Cl[b]	K_2O	CaO	F	Fe_2O_3	CO_2
Na–K–Si											
NKS	39.36		0.42	4.25	0.16	0.07	18.79		0.22		36.73
NKS16	40.18	0.02	1.27	11.19	0.04	0.06	12.74				34.50
7NKS16	25.18	0.12	0.47	15.49			27.76				30.98
9NKS16	27.39		1.11	10.69	0.09		28.13				32.59
Na–K–Ca–Si											
NKCS	45.59		1.04	0.60			11.90	1.65			39.23
NKCS8	37.22		b.d.l.	0.72	b.d.l.	0.05	21.26	2.45			38.29
7NKCS8	23.29		b.d.l.	0.59	0.08	b.d.l.	37.41	2.59			36.05
9NKCS8	24.63	0.11	0.21	3.97	0.20	0.15	33.73	2.05			34.97
NKCS516	37.35	0.09	1.00	12.57	0.17	0.14	14.03	0.83			33.83
Na–K–Ca–Si–F											
NKFS	34.77		b.d.l.	0.48			19.25	4.11	4.49		36.91
NKCFS	35.76		b.d.l.	0.67		b.d.l.	20.25	4.75	4.40		38.58
NKCFS1	33.15		b.d.l.	0.74			19.53	5.05	4.90		36.63
Na–K–Fe–Si											
NKFeS1	45.56	0.17	0.53	1.47	0.09	0.33	12.53			0.44	38.88
NKFeS2	48.81		0.10	0.22		0.08	10.99			b.d.l.	39.79

b.d.l. Below detection limit. Empty cells were not quantified.
a Magnesium oxide introduced from impurities in alumina crucibles.
b Volatile species absorbed from legacy contamination in the furnaces.

Table 3
Compositions of silicate melts.

Run name	Phase	Na_2O	MgO	Al_2O_3	SiO_2	Cl	K_2O	CaO	Fe_2O_3	Totals[b]
NKS	Silicate melt[a]	14.12	0.12	2.73	45.14		13.58			75.69
NKS16	Silicate melt 1	25.47	0.07	5.72	31.69		11.17			74.11
	Silicate melt 2	34.31	0.12	6.24	34.54		15.08			90.29
7NKS16	Silicate melt	7.12	0.12	1.09	34.78	0.14	27.99			71.24
9NKS16	Silicate melt	24.51	0.19	7.52	33.23		19.34			84.79
NKCS516	Silicate melt	28.23		6.81	35.71		14.20	1.37		86.30
NKFeS1	Silicate melt	23.33		2.07	29.00		10.44		33.45	98.29
	Fe-rich melt	18.70		1.18	15.17		8.26		55.88	99.19
NKFeS2	Silicate melt	21.45		2.37	35.37		12.15		20.06	91.40
	Fe-rich melt	11.97	0.64	7.27	26.42		18.85	0.32	31.96	97.43

[a] Occurs as small ~ 20 μm bubbles, likely quench phase and was not present at equilibrium temperature.
[b] Low totals consistent with substantial CO_2 solubility in highly alkaline silicate glasses (Jacobson et al., 2020; Pearce, 1964).

would often be filled with dirt from the cutting process, prior to epoxy resin impregnation, often surrounding kalsilite grains that remained attached to the crucible (Fig. 3c).

All four experiments show substantial silica dissolved in the carbonatite melt. True solubility, as opposed to incidentally trapped equilibrium silicate phases, is demonstrated by the appearance of silica as an integral part of the dendritic quench crystals (alkali carbonates, Fig. 4a–c). The carbonatite melt in the unsaturated 8 % SiO_2 experiment (NKS, marked with an × in Fig. 5a) contained ~ 4.25 % dissolved SiO_2 whereas the saturated 16 % SiO_2 experiments contained between 10.7 % and 15.5 % dissolved SiO_2 (purple circles in Fig. 5a). Contrary to expectations, there was no systematic variation of SiO_2 contents between experiments of different temperatures. This could result from analytical uncertainty owing to heterogenous melt microstructures. Alternatively, we note that carbonatite melts in experiments NKS and NKS16 contained $Na_2O > K_2O$ whereas experiments 7NKS16 and 9NKS16 contained $K_2O > Na_2O$, despite having the same starting composition (Table 2). This could stem from different amounts of kalsilite formation, directly influencing bulk SiO_2 contents available for dissolution in melts, or indirectly by changing melt composition and its equilibrium SiO_2 solubility. Nevertheless, we find that silica solubility in solely alkali carbonatite melts is substantial, and when saturated with an immiscible silicate liquid, can reach double digit numbers of around 10 % to 15 %.

3.2. Na–K–Ca–Si

Following our initial hypothesis, we conducted four experiments (NKCS, NKCS8, 7NKCS8, and 9NKCS8) in which starting $CaCO_3$ exceeded the amount to fully react with SiO_2 to form silicate minerals. Overall, textures resembled the N–K–Si experiments described above, with some differences. Quench dendrites are much shorter and often lack the feathery texture (Fig. 3g, h). None of the experiments contain silicate glass. Instead, they contain combeite (simplified formula: $NaCaSi_3O_9$, see Table 4 for actual compositions), and other chemically related phases. Experiment NKCS8 contains a second silicate phase with stoichiometry roughly equal to $Na_2Ca_2Si_2O_7$, a well-known synthetic compound with a perovskite-like crystal structure (hereafter NCSP; Kahlenberg and Hösch, 2002; Santoso et al., 2022). Both Na–Ca-silicates contained minor K_2O contents (Table 4, cf. Kahlenberg, 2022).

These experiments contained very little silica in the quenched carbonatite melt (orange squares in Fig. 5a), with all but one experiment containing less than 1 % SiO_2. There is a poorly-defined trend of increasing SiO_2 contents with temperature, but for the sub-1 % SiO_2 experiments, the variation is lower than analytical uncertainty. The highest observed SiO_2 contents are around 4 % for experiment 9NKCS8.

Similar to the Na–K–Si experiments, Si is observed in irregular and vermicular patches within the quench dendrites (but at much lower

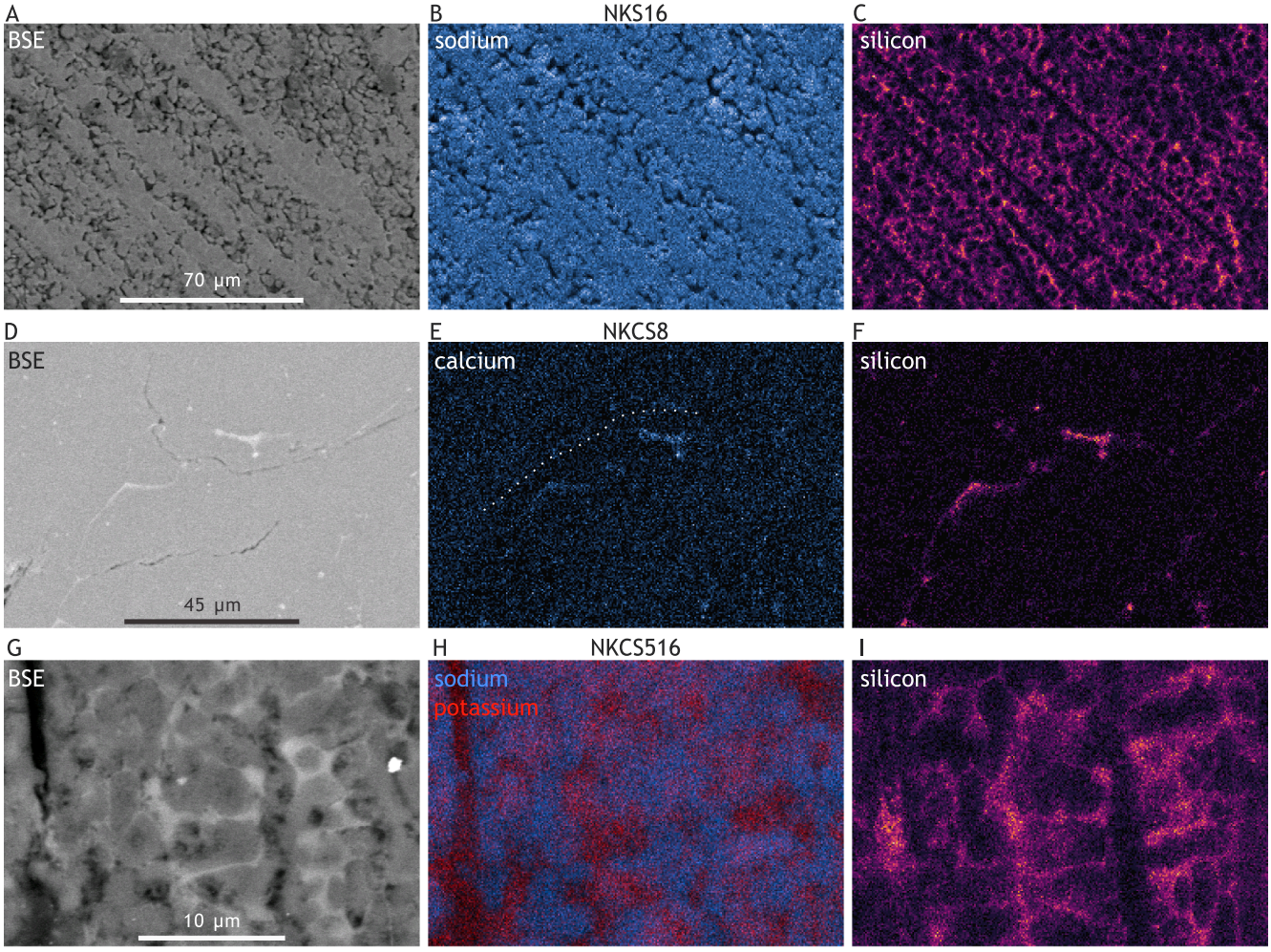

Fig. 4. BSE images (A, D, G) and EDS maps of experiment NKS16 (B, C), NKCS8 (E, F), and NKCS516 (H, I). Sodium and calcium in blue, potassium in red, and silicon in purple. Stronger colours indicate higher counts. Sodium not shown for NKCS8, but dominates field of view. Upper part of the Ca depletion halo around Ca-rich phases in (E) marked with a dotted line.

abundances, Fig. 4d–f), indicating that it was soluble in the melt rather than present as haphazardly trapped equilibrium silicate grains. These patches also contain elevated Ca, with a weak depletion halo around it (Fig. 4e) indicating that during rapid cooling, the Si quench phase sequestered Ca from the surrounding liquid.

An additional experiment, NKCS516, contained much higher SiO_2 compared to its initial $CaCO_3$ contents (Table 1). Our aim was to form Ca–Na-silicates as in previous experiments, but retain leftover SiO_2 in excess of the required amount to react all $CaCO_3$. This is indeed what we discovered in the experimental results, with abundant silicate formation (Fig. 3i, j), and a carbonatite melt that contained ~ 12.6 % SiO_2, but only ~ 0.8 % CaO (Table 2, Fig. 4g–i, starry green triangle in Fig. 5a). The silicate mineral formula is roughly $Na_{3.5}K_{0.5}CaSi_3O_9$, likely to be a potassic solid solution of the known cubic phase $Na_4CaSi_3O_9$ (hereafter, NCSC, Fischer and Tillmanns, 1984; Maki and Sugimura, 1970; Santoso et al., 2022). NCSC occurred in both carbonatite and silicate melts (Figs. 3i, j). When close to the interface between the two liquids, the silicate melt preferentially wets NCSC (Fig. 3j). Several cracks crosscut the silicate liquid with its NCSC crystals, but they are filled with carbonate material. We suspect this occurred during quenching, when thermal shock cracked the silicate material and the still-liquid carbonatite melt rapidly flowed to fill the void (Fig. 3j).

3.3. *Na–K–Ca–Si–F*

So far, carbonate was the only anion in our experiments. Next, we conducted experiments in which some $CaCO_3$ was replaced on a mole-by-mole basis with CaF_2. This was done for several reasons. First, fluorine is known to change carbonatite melt properties (Berkesi et al., 2020; Jago and Gittins, 1991; Weidendorfer et al., 2017; Xue et al., 2024). Second, we wished to explore the effect of CO_2 dilution within the melt. For our reasoning, we started with the basic decarbonation reaction

$$\underset{\text{calcite}}{CaCO_{3(l)}} + \underset{\text{silica}}{SiO_{2(l)}} = \underset{\text{wollastonite}}{CaSiO_{3(s)}} + \underset{\text{gas}}{CO_{2(g)}}.$$

We hypothesised that lowering $CaCO_3$ activity would stabilise additional silica within the melt via Le Chatelier's principle, whereby wollastonite in the simplified reaction represents a saturated silicate phase (e.g., combeite), and CO_2 remains fixed by furnace atmosphere control. Finally, F^- in calcic environments is typically non-volatile and is more likely to fully remain within the crucible during long-duration experiments. This contrasts with other anions typical for carbonatites such as Cl^- or SO_4^{2-}, which are much more volatile (in fact, they were absorbed *into* the liquids from legacy furnace contamination during some experimental runs, Table 2).

The results were mostly similar to the Na–K–Ca–Si experiments, with

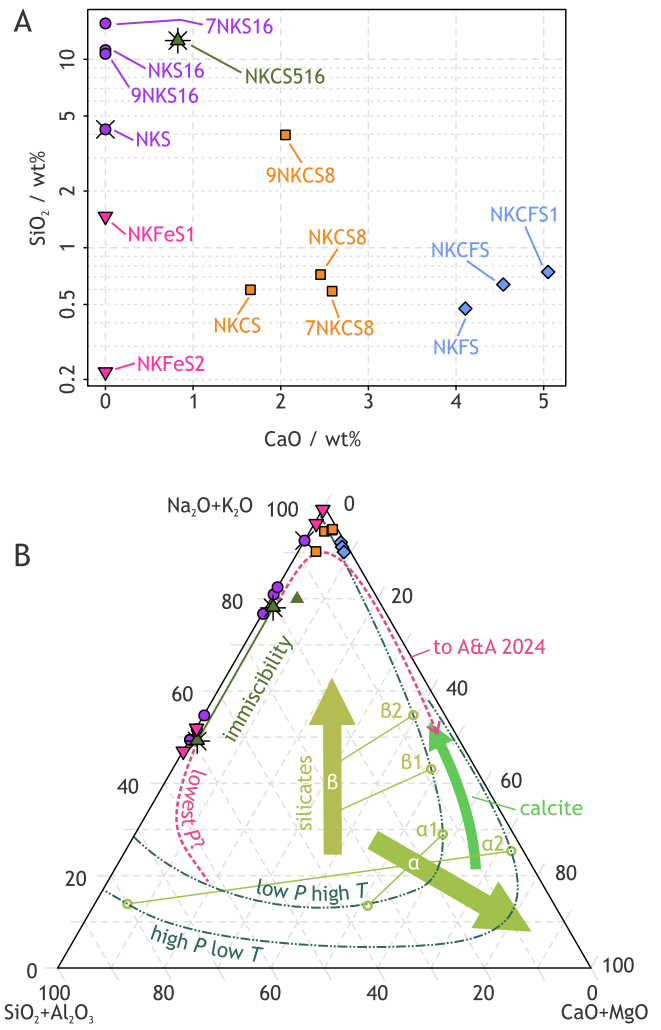

Fig. 5. Chemical compositions of experimental liquids from Table 2 and 3. (A) CaO vs SiO_2 of quenched carbonatite melts from all experiments. SiO_2 plotted in logarithmic scale. (B) Coexisting carbonatite and silicate compositions plotted on a ternary carbonatite projection. Quenched carbonatite melts plot at ≥80 % alkalis, whereas silicate glasses cluster close to 50 % alkalis. Dashed-dotted lines show typical variation of carbonatite–silicate immiscibility curves as a function of pressure (*P*) and temperature (*T*), loosely based on (Brooker and Kjarsgaard, 2011). Pink dashed line starting at the silicate cluster shows hypothetical continuation of the immiscibility curve at 1 bar, if it were stable. Pink dashed line starting at the carbonatite cluster shows range of possible carbonatite melt compositions at 1 bar. Trend to higher CaO compositions observed in the related 1 bar experiments of Anenburg and Aslam (2024). Green tie-line connects the two immiscible liquids of run NKCS516 (starry green triangle, starting composition for this run is given by the non-starry triangle). Olive green arrow and associated tie-lines (α) show compositional evolution with decreasing temperature. Grass green arrow shows compositional evolution with calcite fractionation. Khaki line and associated half tie-lines (β) show compositional evolution with antiskarn-type silicate crystallisation.

dendritic carbonatite melts, combeite, occasional NCSP, and kalsilite coating the interior of the alumina crucible. Combeite grains were notably larger than in the F-free experiments, demonstrating the fluxing effect of fluorine in carbonatite melt (Fig. 3k). We point out that these coarser combeite crystals look remarkably like combeite found in Oldoinyo Lengai, a natural F-rich natrocarbonatite volcano (see combeite gallery at mindat.org; https://www.mindat.org/gm/1115). Fluorine was wholly soluble in the melt with no observed fluorite, immiscible fluoride melt, or detectable F contents in any of the solid phases. Silica contents were low; all three experiments had less than 1 % SiO_2 (blue diamonds in Fig. 5a, Table 2). Carbonatite melt often quenched to a distinct vermicular intergrowth (Fig. 3l), unlike typical carbonatite quench forms being mostly straight dendrites. In larger liquid areas, the vermicules formed part of large feather microstructures with curved barbs.

3.4. *Na–K–Fe^{3+}–Si*

We attempted to explore the behaviour of a cation other than Ca. The obvious candidate was magnesium, a common element in carbonatite-hosted silicates, abundant in clinopyroxenes, amphiboles, olivine, and micas. However, $MgCO_3$ has poor thermal stability and was not suitable for our 1 atmosphere experiments as it would precipitate out as periclase (Stone, 1954), a rare mineral not typical of carbonatites. Divalent iron faces similar issues, and would not be stable in our oxidising CO_2 atmosphere. However, Fe^{3+} is stable in CO_2 atmospheres, and is a major component of common carbonatite-associated silicates, with aegirine being the most typical example. Any insoluble Fe^{3+} excess would presumably precipitate out as magnetite or hematite. We conducted two experiments, first running NKFeS1 at 850 °C in which no well-defined solid phases formed (Fig. 3m). In order to assist formation of Fe^{3+}-bearing silicates, we cooled experiment NKFeS2 to 600 °C from 850 °C to (1) form liquid silicate pools that would coarsen by coalescing, and (2) crystallise solids out of them (ideally aegirine) by crossing the liquidus.

This experiment resulted in carbonatite–silicate immiscibility similar to previous experiments (Fig. 3n). Kalsilite occurred both as a coating on the alumina crucible, and as phenocrysts within the silicate liquid. Kalsilite was markedly ferric, with substantial Fe^{3+} replacing Al^{3+} in its crystal structure. The carbonatite melt contained low SiO_2 up to ~ 1.5 % (pink inverted triangles in Fig. 5a), and surprisingly low Fe_2O_3 content up to 0.44 % (Table 2). An additional Fe-rich phase was present within the silicate melt. It is not glassy and has amoeboid outlines, characteristic of a liquid (Fig. 3o, Table 3). Although difficult to confirm, we suspect that it was a third immiscible liquid as often happens in Fe-rich silicate melts (Thompson et al., 2007).

Despite our attempts to crystallise aegirine, none was formed. Instead, Fe^{3+} was sequestered in kalsilite. Nevertheless, we expect that if the experiment had cooled below 600 °C, aegirine would have formed because the liquid compositions were not too far off from aegirine compositions (Table 3).

4. Discussion

Our results show that SiO_2 and CaO are mostly mutually exclusive in our carbonatite melts. High SiO_2 contents of the carbonatite melt were only found in Ca-free experiments, or when Ca was present but at merely 0.83 % CaO (experiment NKCS516, starry green triangle in Fig. 5a). All but one other Ca-bearing experiments contained up to 0.7 % SiO_2. It is unclear what caused experiment 9NKCS8 to have ~ 4 % SiO_2. Care was taken during analysis to avoid silicates while rastering, and these values were consistent across several measured areas. It could potentially derive from its higher temperature of 950 °C, but such a drastic increase of 3 % SiO_2 across a temperature increase of 100 °C seems excessive, given previously-derived temperature–composition relationships (Schmidt et al., 2024). Nevertheless, even at 4 % SiO_2, it is substantially lower than the Ca-free and silicate saturated experiments consisting of > 10 % SiO_2 and an immiscible silicate melt (Fig. 5a).

We find that given the co-introduction of CaO and SiO_2 into our carbonatite melts, they will react with each other to precipitate a sodic calcium silicate (Fig. 3) until either CaO or SiO_2 is exhausted. Then, the other component would remain soluble in the carbonatite melt. Essentially, they will titrate themselves out of the carbonatite melt.

Kalsilite also records some degree of silica insolubility aided by Al_2O_3, whereby its formation removed some SiO_2 from the carbonatite melt. Despite having a potentially abundant—essentially

Table 4
Mineral compositions.

Run name	Na_2O	K_2O	CaO	MgO	Fe_2O_3[a]	Al_2O_3	SiO_2	Totals[b]	Na	K	Ca	Mg	Fe	Al	Si
	weight percent								atoms per formula unit						
kalsilite (nominally $KAlSiO_4$)															
NKS	4.24	24.92				35.26	35.26	106.27	0.20	0.77			0.00	1.00	1.01
NKS16	3.02	25.76				32.12	32.12	99.615	0.15	0.86			0.00	0.99	1.01
7NKS16	1.01	27.64		0.3[c]		30.42	30.42	97.04	0.05	0.95			0.00	0.97	1.02
9NKS16	1.98	27.53				32.37	32.37	100.83	0.10	0.91			0.00	0.99	1.01
NKCS8	4.73	24.52			0.40	36.11	36.11	110.05	0.21	0.72			0.01	0.98	1.02
9NKCS8	2.49	27.42		0.87[c]		29.13	29.13	95.59	0.14	0.98			0.00	0.96	1.00
NKFeS2 core	1.26	25.61			22	15.28	15.28	97.28	0.07	0.96			0.49	0.53	0.98
NKFeS2 rim	2.14	24.16			31.52	8.98	8.98	97.54	0.13	0.95			0.73	0.32	0.94
combeite (nominally $Na_2Ca_2Si_3O_9$)															
NKCS8	24.36	0.58	24.915			0.39	52.03	102.28	2.73	0.04	1.55			0.03	3.01
NKFS	22.64333	0.556667	25.36667			0.21	50.60667	99.39	2.62	0.04	1.62			0.01	3.01
NKCFS	22	0.865	25.36			0.14	50.295	98.66	2.56	0.07	1.63			0.01	3.02
NKCFS1	22.16	0.6	24.92			0.29	50.02	97.99	2.59	0.05	1.61			0.02	3.02
NCSP (nominally $Na_2Ca_2Si_2O_7$)															
NKCS	18.65	0.93	38.78			0.14	39.33	97.83	1.82	0.06	2.09	0.00		0.01	1.98
NKCS8	19.495	1.22	36.50	0.19		0.36	40.87	98.635	1.87	0.08	1.94	0.01		0.02	2.02
9NKCS8	15.83	4.12	35.20	0.19			36.80	92.14	1.66	0.28	2.04	0.02		0.00	1.99
NKCFS	17.91	1.32	36.65	0.2		0.07	38.79	94.94	1.79	0.09	2.03	0.02		0.00	2.00
NKCFS1	18.6	1.23	38.35	0.24			41.04	99.46	1.77	0.08	2.02	0.02		0.00	2.02
NCSC (nominally $Na_4CaSi_3O_9$)															
NKCS516	30.07	5.28	15.00				49.74	100.09	3.54	0.41	0.98				3.02

a All iron calculated as Fe_2O_3, but at the high fO_2 conditions of our experiment we expect to be very little, if any, FeO present.
b Totals occasionally differed from 100%. We suspect this to result from irregularities in carbon coating thickness and charging-induced beam deflection caused by the porous nature of nonideal polished samples.
c MgO not included in kalsilite stoichiometry.

"infinite"—supply of crucible-derived Al_2O_3, the reaction was limited in scale and primarily confined to the liquid–crucible interface (Fig. 3c). We suspect that kalsilite formation passivated the alumina crucible, armouring it from the carbonatite melt and preventing further reaction. This is supported by experiment NKFeS2, where exceptionally Fe-rich kalsilite was found within the two liquids, indicating that the mineral is generally stable, but did not have sufficient supply of trivalent cations in Fe-free experiments. Crucible passivation is further demonstrated by kalsilite zoning to Fe-rich rims, recording the depletion of available Al_2O_3 (Fig. 3n).

Our results provide a straightforward explanation for quartz crystallisation observed in the Yuan et al. (2024) experiments. A visual assessment of their figures shows that quartz consisted of between 10 % and 20 % of their initial starting volume. A rough estimate of the final volume fraction indicates up to about 15 % quartz. Most of their quartz reacted at high temperatures to form the silicates britholite and aegirine. This reaction also removed all non-alkali metals from the liquid, leaving behind a liquid that predominantly contained H_2O, Na_2CO_3, and minor SiO_2. A purely sodic liquid, as seen in our experiments, can easily dissolve substantial SiO_2 and that was indeed the case for Yuan et al. (2024). During final cooling, this SiO_2 precipitated as quartz; it had no other non-alkali metals left in the liquid to react with to form other silicate minerals. Their experiments were K-free, hydrous, and conducted at elevated pressure, so a direct comparison of solubilities and stable mineral assemblages cannot be made, but the overall trend remains. We note that they did not crystallise any combeite, instead forming cancrinite: a K-free carbonated Na–Ca-aluminosilicate, consistent with their non-potassic compositions and high pressures of several kilobars (also synthesised by Watkinson and Wyllie, 1971).

4.1. Shape and disappearance of the miscibility gap

The carbonatite–silicate miscibility gap is well characterised across a range of compositions, temperatures, and pressures (Berkesi et al., 2020; Schmidt et al., 2024; Yaxley et al., 2021). Broadly speaking, the gap narrows with lower pressures and higher temperatures (Brooker and Kjarsgaard, 2011), leading to increasing mutual solubilities of carbonatite and silicate components (Fig. 5b). Our ~1 bar experiments extend the known pressure trend as expected: the immiscible melts plot closer to each other than previously determined for higher pressures. Importantly, the immiscible silicate and carbonatite melts consistently plot in the same place on the ternary in Fig. 5b, demonstrating reproducibility across several experiments with variable compositions and temperatures.

Our two liquids are located near the alkali–network-former edge of the ternary (i.e., Na_2O + K_2O–SiO_2 + Al_2O_3, Fig. 5b). Calcium was poorly soluble in all experimental melts, despite being present in the experiments. Any attempts to add CaO to the system resulted in its rejection from the liquids. Instead, CaO was sequestered in silicate minerals, forcing the tie-line back to its observed position along the ternary edge. In contrast, previous work at higher pressures always succeeded in having immiscible liquids with tie-lines that cross the ternary interior (Berkesi et al., 2020; Brooker and Kjarsgaard, 2011; Guzmics et al., 2011; Schmidt et al., 2024). We suggest this might be an important characteristic of low-pressure immiscibility in silicate–carbonatite systems. Consequently, the pink dashed line in Fig. 5b is not a true solvus or binodal curve. Instead, it encloses a forbidden zone for liquid compositions. The presence of silicate is important for this to occur. Addition of CaO to a silicate-free system, even in 1 bar, results in increasing CaO contents of the carbonatite melt, up to calcite saturation (Anenburg and Aslam, 2024). Calcic silicates (e.g., combeite) could hypothetically dissolve into either or both liquids at higher temperatures. However, carbonate is only stable at sufficiently low temperatures; higher temperatures would lead to CO_2 degassing and carbonate decomposition—two of our runs were at 950 °C, already above the calcite decomposition point. This means that the large two-liquid fields typical of silicate–carbonate ternary diagrams (Yaxley et al., 2021) do not exist in surface conditions. They are metastable with respect to (1)

loss of Ca to silicates, pushing the bulk composition away from the CaO apex, and (2) CO_2-loss, shrinking the miscibility gap as was previously observed at high pressure by Brooker and Kjarsgaard (2011).

The alkali enrichment of both liquids with decreasing pressure as inferred from our experiments could be a contributing factor to the unusual alkali-rich character of the Oldoinyo Lengai carbonatite lavas and associated combeite nephelinites (Guzmics et al., 2019; Sharygin et al., 2012). Further evidence is provided by formation of combeite in reaction rims around wollastonite and pyroxene in Oldoinyo Lengai (Dawson et al., 1989). Curiously, only combeite was found in nature (hence it being given a mineral name), whereas NCSP and NCSC were not. We speculate that these minerals might exist in similar geological environments, as only small bulk compositional variations are required to stabilise one or the other (Santoso et al., 2022). Whether they have been found but misidentified as combeite due to their chemical similarities, or have simply yet to be unearthed by a qualified mineralogist, is unknown.

4.2. Relevance for natural carbonatite formation and evolution

Carbonatites are typically dominated by calcite or dolomite, as these are the common cumulate minerals, whereas alkali components are not preserved in the geological record despite evidence for their former occurrence (Anenburg and Aslam, 2024; Yaxley et al., 2022). Typical carbonatite differentiation paths based on naturally-observed and experimentally-derived liquid lines of descent show that even mildly evolved carbonatite melts are sufficiently alkaline to drive silica solubility to single-digit figures (Guzmics et al., 2011; Guzmics et al., 2012; Weidendorfer et al., 2017). In both our experiments and those of Yuan et al. (2024), notable silica solubility was observed in purely alkali carbonatite melts. But are such liquids widespread in nature? We would argue that they are not, unless exceptional circumstances are met. Carbonatite compositions close to the CaO apex in compositional ternary diagrams will initially form during silicate–carbonatite immiscibility or magmatic differentiation (Lee and Wyllie, 1998a). The solvus curvature in this region is wide (Brooker and Kjarsgaard, 2011; Schmidt et al., 2024), such that many carbonatite melts can contain up to about 15 % SiO_2, particularly at temperatures higher than about 1000 °C (Fig. 5b, see also Zech et al., 2025). However, once the carbonatite melts separate from their conjugate silicate melts (typically after some degree of mutual fractionation, Guzmics et al., 2012; Lee and Wyllie, 1998a), they will rapidly evolve to compositions that only permit strongly decreasing silica solubility. This is achieved via three processes, working in tandem. First, temperature decrease widens the miscibility gap and sharpens the solvus curve, effectively removing SiO_2 from the carbonatite melt (α in Fig. 5b). Second, this removal is primarily achieved by crystallisation of calcic silicates such as clinopyroxene (Anenburg and Walters, 2024). This pushes the melt composition towards the alkali apex into solvus sections with strongly diminishing silica solubility (β in Fig. 5b). This may act as positive feedback where calcic silicates are forming, only to drive the solvus further away from the SiO_2 apex, triggering additional formation of calcic silicates. Thirdly and importantly, calcite is the predominant crystallising phase during cooling (Guzmics et al., 2011; Lee and Wyllie, 1998b, 2000; Weidendorfer et al., 2017), and its fractionation strongly controls melt composition and drives evolution along the SiO_2-poor solvus (Fig. 5b, also see Anenburg and Aslam, 2024). Silica solubility then becomes entirely negligible somewhere in the range of 1000 °C and 900 °C. This temperature range is typically the upper formation limit for many carbonatites (Berkesi et al., 2023; Guzmics et al., 2012; Schmidt et al., 2024).

Carbonatites often occur in ring complexes, with carbonatites in their cores and silicate-dominated rocks in their peripheries. In some cases, these silicates were explained as cumulates forming by silicate crystallisation from a carbonated silicate melt or the carbonatite melt itself. In this model, silica is substantially soluble in carbonatite melts and silicocarbonatite magmas are proposed to exist (Ackerman et al., 2021; Beccaluva et al., 1992; Doroshkevich et al., 2017; Moore et al., 2022; Ryabchikov and Kogarko, 2016; Veksler et al., 1998). However, in many cases the carbonatites are volumetrically dwarfed by the surrounding silicate rocks (Vasyukova and Williams-Jones, 2022). Silica solubilities from our experiments and those derived from literature data discussed above are too small to explain such voluminous cumulates. In some cases where endogenous silicate phenocryst formation was observed in carbonatites, their volumes were accordingly very small (Li et al., 2024). Recently, alternative hypotheses have suggested that these rocks form by metasomatic reaction between carbonatite melts and their host silicate rocks (Anenburg and Walters, 2024; Vasyukova and Williams-Jones, 2022). Our findings provide further support for this metasomatic model, whereby the silica is externally supplied and may results in abundant silicate crystallisation within the igneous body.

4.3. Implications for ore-forming carbonatite systems

Silica has been suggested to play a role in carbonatite-associated ore formation, with a particular focus on REE. The Yuan et al. (2024) experiments were specifically designed to observe REE behaviour in carbonatitic brine-melts. Their finding of substantial SiO_2 solubility and quartz formation has potential implications for other formation models. For example, Cui et al. (2020) suggested that silica enhances REE mobility in sulfate-rich fluids, such as those commonly observed in carbonatite-hosted fluid inclusions. Huang et al. (2023) proposed a role for Si–F complexes in REE mineralisation. Zhang et al. (2022) highlighted the presence of quartz in carbonatite complexes and speculated on its role in REE ore formation.

For these silica-driven suggested processes to have an impact on ore-formation, SiO_2 must actually be soluble in carbonatite melts, and be available to partition to any ore-forming hydrothermal fluids that allegedly exsolve from said carbonatite melts. This has been assumed for these studies (Cui et al., 2020; Huang et al., 2023; Zhang et al., 2022), but not yet demonstrated. We argue that this assumption is unfounded. As described in section 4.1 above, shortly after initial carbonatite differentiation, silica solubility becomes negligible. However, REE enrichment in residual brine-melts and subsequent mineralisation requires protracted fractionation of calcite and, in many cases, dolomite. Mororó et al. (2024), for example, showed no silica solubility in REE-bearing fluid inclusions, despite being hosted in quartz. Hence, the two required chemical features (firstly presence of silica, and secondly REE enrichment) for silica-based mineralisation models are separated temporally and probably spatially. They are placed at opposite ends of the carbonatite differentiation sequence; by the time REE are sufficiently enriched to form economic minerals, endogenous silica is long gone from the melt. In these cases, the only way for the melt to gain silica is by assimilation from the country rocks. However, since the solubility is so low, any significant SiO_2 is never dissolved in the melt nor is it transported to any notable distance. Instead, it immediately reacts with carbonatite-derived elements to form an antiskarn (similar to kalsilite and combeite formation in our experiments). Silica can only accumulate as a dissolved species in the melt if all non-alkali cations are exhausted and the melt remains purely alkaline with respect to major element composition. Whether this occurs in nature to any substantial extent is questionable. As antiskarns most often form on carbonatite conduit walls (Anenburg and Mavrogenes, 2018; Anenburg et al., 2020a; Bouabdellah et al., 2022; Chmyz et al., 2022, 2025; Liu and Anenburg, 2025; Xiao et al., 2025), progressive antiskarnisation will armour the carbonatite and prevent efficient silica assimilation from the wall rocks. This process is mirrored in our experiments as well, where kalsilite primarily formed on the capsule walls, despite having no shortage of bulk Al_2O_3, K_2O, and SiO_2 to form copious amounts of kalsilite. The above discussion demonstrates that notable SiO_2 contents are unlikely to exist in late stage brine-melts, nor in any derived or exsolved hydrothermal fluids. We have no objection to localised pockets of carbonatite melt which succeeded in complete reaction with their host rocks to the

degree that any additional silica contamination leads to effective dissolution in the melt. However, carbonatite melts have notoriously low viscosities and rapid diffusion rates (Kono et al., 2014; Stagno et al., 2018) such that the presence of isolated melt pockets is probably rare and short-lived. Even if such silica-involving mineralisation processes do exist, we argue that they are not the dominant or controlling process in mineralised REE deposits.

In the Zhang et al. (2022) review, they found that carbonatite-hosted quartz is typically low in trace elements. They noted that this trace element signature is distinct from the signature of many ore-forming systems, and suggested a model for hydrothermal quartz formation in carbonatites. As discussed previously, for this to occur, silica has to be soluble in the carbonatite melt and derive from it. Our analysis shows that this is not the case. The low trace element signature observed by Zhang et al. (2022) is consistent with that of many sedimentary and metamorphic environments (Götze, 2012; Monecke et al., 2002). We suggest that this carbonatite-hosted quartz is, in fact, metamorphic—in the sense that it formed as post-magmatic silica-bearing ambient fluids precipitated quartz in vugs and cavities inside the carbonatite. These cavities are expected, given that late-stage brine-melts crystallise into a water-soluble assemblage of alkali salts (Anenburg et al., 2020b; Yuan et al., 2023, 2024). Therefore, quartz is likely to be replacing those salts and is unrelated to any REE mineralisation, which was already in place before quartz formation (see additional discussion by Liu and Anenburg, 2025).

5. Summary

Our study demonstrates that SiO_2 and CaO will titrate each other out of alkali-bearing carbonatite melts and deposit as refractory calcium silicates (e.g., combeite in our case) until one is exhausted. In the presence of Al_2O_3, kalsilite can also form, contributing to lower SiO_2 contents. Silica is only significantly soluble if no other cations are present to sequester SiO_2 into insoluble minerals, namely the non-alkali metals.

In natural carbonatite melts, silica is only soluble to notable amounts for a short temperature interval at the early stages of carbonatite differentiation. This indicates that voluminous silicate rocks associated with carbonatites are highly unlikely to form by fractionation from the carbonatite melt. Elsewhere, silicocarbonatites and any other silicate assemblages within carbonatites are probably antiskarns, formed by reaction of carbonatite-derived metal cations with exogenous silica. Previously hypothesised low-temperature and silica-driven mineralisation processes for carbonatite-hosted ore deposits may need to be reassessed.

At our conditions of atmospheric pressure and 750–950 °C, liquid immiscibility is restricted to the SiO_2–alkali-dominated edge of the carbonatite ternary, away from the CaO-rich apex. Any addition of non-alkali metals triggers solid mineral formation, instead of metal dissolution in the liquids. This could explain some aspects of the alkali-rich compositions of erupted carbonatites and associated rocks, including recent activity at Oldoinyo Lengai and elsewhere in the geological record.

Data availability

All data are provided in the manuscript. Raw data and calculations are available through figshare at https://doi.org/10.6084/m9.figshare.30335911.v1.

CRediT authorship contribution statement

Xinxiang Zhu: Investigation, Formal analysis, Writing – review & editing. **Michael Anenburg:** Writing – review & editing, Writing – original draft, Supervision, Conceptualization, Methodology, Visualization. **Yan Liu:** Writing – review & editing, Funding acquisition.

Declaration of competing interest

The authors declare that they have no known competing financial interests or personal relationships that could have appeared to influence the work reported in this paper.

Acknowledgments

This work was supported by the National Science and Technology Major Project (2025ZD1004808), National Natural Science Foundation of China (Grant No. 42521002), and Baotou Research Institute of Rare Earths Project (2025Z2629). Tibor Guzmics provided useful suggestions on an earlier version of the manuscript. Tahar Hammouda and Dima Kamenetsky contributed reviews which helped clarify and improve our work, and Olivier Namur provided valuable editorial support. David Clark assisted with technical support in the experimental lab. The authors acknowledge Microscopy Australia (ROR: 042mm0k03) at the Centre for Advanced Microscopy, The Australian National University, a facility enabled by NCRIS and university support.

References

Ackerman, L., Rapprich, V., Polák, L., Magna, T., McLemore, V.T., Pour, O., Čejková, B., 2021. Petrogenesis of silica-rich carbonatites from continental rift settings: a missing link between carbonatites and carbonated silicate melts? J. Geosci. 66 (2), 71–87.
Anenburg, M., Aslam, I.N., 2024. Calcite-saturated natrocarbonatites: composition, crystal morphology, and weathering. Volcanica 7 (2), 813–833.
Anenburg, M., Guzmics, T., 2023. Silica is unlikely to be soluble in upper crustal carbonatite melts. Nat. Commun. 14 (1), 942.
Anenburg, M., Mavrogenes, J.A., 2018. Carbonatitic versus hydrothermal origin for fluorapatite REE-Th deposits: experimental study of REE transport and crustal "antiskarn" metasomatism. Am. J. Sci. 318 (3), 335–366.
Anenburg, M., Mavrogenes, J.A., Bennett, V.C., 2020a. The fluorapatite P–REE–Th vein deposit at Nolans Bore: Genesis by carbonatite metasomatism. J. Petrol. 61 (1), egaa003.
Anenburg, M., Mavrogenes, J.A., Frigo, C., Wall, F., 2020b. Rare earth element mobility in and around carbonatites controlled by sodium, potassium, and silica. Sci. Adv. 6 (41), eabb6570.
Anenburg, M., Walters, J.B., 2024. Metasomatic ijolite, glimmerite, silicocarbonatite, and antiskarn formation: carbonatite and silicate phase equilibria in the system Na_2O–CaO–K_2O–FeO–MgO–Al_2O_3–SiO_2–H_2O–O_2–CO_2. Contrib. Miner. Petrol. 179 (5), 40.
Beccaluva, L., Barbieri, M., Born, H., Brotzu, P., Coltorti, M., Conte, A., Garbarino, C., G, C.B.G., M, A., Morbidelli, L., Ruberti, E., Siena, F., Traversa, G., 1992. Fractional crystallization and liquid immiscibility processes in the alkaline-carbonatite complex of Juquiá (São Paulo, Brazil). J. Petrol. 33 (6), 1371–1404.
Berkesi, M., Bali, E., Bodnar, R.J., Szabó, Á., Guzmics, T., 2020. Carbonatite and highly peralkaline nephelinite melts from Oldoinyo Lengai Volcano, Tanzania: the role of natrite-normative fluid degassing. Gondw. Res. 85, 76–83.
Berkesi, M., Myovela, J.L., Yaxley, G.M., Guzmics, T., 2023. Carbonatite formation in continental settings via high pressure – high temperature liquid immiscibility. Geochim. Cosmochim. Acta 349, 41–54.
Berndt, J., Klemme, S., 2022. Origin of carbonatites—liquid immiscibility caught in the act. Nat. Commun. 13 (1), 2892.
Berndt, J., Klemme, S., 2023. Reply to: Silica is unlikely to be soluble in upper crustal carbonatite melts. Nat. Commun. 14 (1), 943.
Bouabdellah, M., Boukirou, W., Jébrak, M., Bigot, F., Yans, J., Mouttaqi, A., El Gadarri, M., Errami, A., Levresse, G., 2022. Discovery of antiskarn-hosted strategic metal mineralization in the Upper cretaceous Twihinate carbonatite intrusion (West African Craton Margin, Moroccan Sahara). Ore Geol. Rev. 149, 105105.
Brooker, R.A., Kjarsgaard, B.A., 2011. Silicate–carbonate liquid immiscibility and phase relations in the system SiO_2–Na_2O–Al_2O_3–CaO–CO_2 at 0.1–2.5 GPa with applications to carbonatite genesis. J. Petrol. 52, 1281–1305.
Chayka, I.F., Kamenetsky, V.S., Vladykin, N.V., Kontonikas-Charos, A., Prokopyev, I.R., Stepanov, S.Y., Krasheninnikov, S.P., 2021. Origin of alkali-rich volcanic and alkali-poor intrusive carbonatites from a common parental magma. Sci. Rep. 11 (1), 17627.
Chebotarev, D.A., Veksler, I.V., Wohlgemuth-Ueberwasser, C., Doroshkevich, A.G., Koch-Müller, M., 2019. Experimental study of trace element distribution between calcite, fluorite and carbonatitic melt in the system $CaCO_3 + CaF_2 + Na_2CO_3 \pm Ca_3(PO_4)_2$ at 100 MPa. Contrib. Miner. Petrol. 174 (1), 4.
Chmyz, L., Azzone, R.G., Ruberti, E., Guarino, V., 2025. Wall rock assimilation in carbonatite magmas: Textural, mineral and whole-rock geochemical signatures in the Jacupiranga complex, Brazil. Geochemistry 85 (1), 126218.
Chmyz, L., Azzone, R.G., Ruberti, E., Marks, M.A.W., Santos, T.J.S.d., 2022. Olivines as probes into assimilation of silicate rocks by carbonatite magmas: Unraveling the genesis of reaction rocks from the Jacupiranga alkaline-carbonatite complex, southern Brazil. Lithos 416–417, 106647.

Çubukçu, H.E., Ersoy, O., Aydar, E., Çakir, U., 2008. WDS versus silicon drift detector EDS: a case report for the comparison of quantitative chemical analyses of natural silicate minerals. Micron 39 (2), 88–94.
Cui, H., Zhong, R., Xie, Y., Yuan, X., Liu, W., Brugger, J., Yu, C., 2020. Forming sulfate- and REE-rich fluids in the presence of quartz. Geology 48 (2), 145–148.
Dawson, J.B., 1962. Sodium carbonate lavas from Oldoinyo Lengai, Tanganyika. Nature 195 (4846), 1075–1076.
Dawson, J.B., Smith, J.V., Steele, I.M., 1989. Combeite ($Na_{2.33}Ca_{1.74}others_{0.12})Si_3O_9$ from Oldoinyo Lengai, Tanzania. J. Geol. 97 (3), 365–372.
Doroshkevich, A.G., Veksler, I.V., Klemd, R., Khromova, E.A., Izbrodin, I.A., 2017. Trace-element composition of minerals and rocks in the Belaya Zima carbonatite complex (Russia): implications for the mechanisms of magma evolution and carbonatite formation. Lithos 284–285, 91–108.
Fischer, R.X., Tillmanns, E., 1984. Die Kristallstruktur von $Na_4CaSi_3O_9$ und dessen strukturelle Beziehungen zu $K_4SrGe_3O_9$ und $Ca_3Al_2O_6$. Zkri 166 (1–4), 245–256.
Gales, E., Black, B., Elkins-Tanton, L.T., 2020. Carbonatites as a record of the carbon isotope composition of large igneous province outgassing. Earth Planet. Sci. Lett. 535, 116076.
Giebel, R.J., Parsapoor, A., Walter, B.F., Braunger, S., Marks, M.A.W., Wenzel, T., Markl, G., 2019. Evidence for magma–wall rock interaction in carbonatites from the Kaiserstuhl Volcanic complex (Southwest Germany). J. Petrol. 60 (6), 1163–1194.
Götze, J., 2012. Classification, mineralogy and industrial potential of SiO_2 minerals and rocks, Quartz: Deposits, Mineralogy and Analytics. pp. 1–27.
Guo, H., Tuduri, J., Nabyl, Z., Erdmann, S., Li, X., Gaillard, F., 2024. Rare earth elements in apatite: a proxy for unravelling carbonatite melt compositions. Earth Planet. Sci. Lett. 642, 118863.
Guzmics, T., Berkesi, M., Bodnar, R.J., Fall, A., Bali, E., Milke, R., Vetlényi, E., Szabó, C., 2019. Natrocarbonatites: a hidden product of three-phase immiscibility. Geology 47 (6), 527–530.
Guzmics, T., Mitchell, R.H., Szabó, C., Berkesi, M., Milke, R., Abart, R., 2011. Carbonatite melt inclusions in coexisting magnetite, apatite and monticellite in Kerimasi calciocarbonatite, Tanzania: Melt evolution and petrogenesis. Contrib. Miner. Petrol. 161 (2), 177–196.
Guzmics, T., Mitchell, R.H., Szabó, C., Berkesi, M., Milke, R., Ratter, K., 2012. Liquid immiscibility between silicate, carbonate and sulfide melts in melt inclusions hosted in co-precipitated minerals from Kerimasi volcano (Tanzania): evolution of carbonated nephelinitic magma. Contrib. Miner. Petrol. 164 (1), 101–122.
Huang, Y.-S., Liu, Q., Liu, F.-X., Li, X.-C., Liu, Y., Tang, G.-Q., Fan, H.-R., Li, X.-H., Li, Q.-L., 2023. Large Si isotope fractionation reveals formation mechanism of quartz in silicon-poor carbonatite. Geology 51 (11), 1038–1042.
Jacobson, N.S., Fegley, B., McAdam, A.C., Knudson, C.A., 2020. Solubility of CO_2 in sodium silicate melts. ACS Earth Space Chem. 4 (11), 2113–2120.
Jago, B.C., Gittins, J., 1991. The role of fluorine in carbonatite magma evolution. Nature 349 (6304), 56–58.
Kahlenberg, V., 2022. Concerning the incorporation of potassium in the crystal structure of combeite ($Na_2Ca_2Si_3O_9$). Mineral. Petrol. 117 (2), 293–306.
Kahlenberg, V., Hösch, A., 2002. The crystal structure of $Na_2Ca_2Si_2O_7$ - a mixed anion silicate with defect perovskite characteristics. Zkri 217 (4), 155–163.
Kamenetsky, V.S., Doroshkevich, A.G., Elliott, H.A.L., Zaitsev, A.N., 2021. Carbonatites: contrasting, complex, and controversial. Elements 17 (5), 307–314.
Kjarsgaard, B.A., 1998. Phase relations of a carbonated high-CaO nephelinite at 0.2 and 0.5 GPa. J. Petrol. 39 (11–12), 2061–2075.
Kono, Y., Kenney-Benson, C., Hummer, D., Ohfuji, H., Park, C., Shen, G., Wang, Y., Kavner, A., Manning, C.E., 2014. Ultralow viscosity of carbonate melts at high pressures. Nat. Commun. 5, 5091.
Le Maitre, R.W., Streckeisen, A., Zanettin, B., Le Bas, M.J., Bonin, B., Bateman, P., 2002. Igneous Rocks: A Classification and Glossary of Terms, 2nd edition. Cambridge University Press, Cambridge.
Lee, W.-J., Wyllie, P.J., 1994. Experimental data bearing on liquid immiscibility, crystal fractionation, and the origin of calciocarbonatites and natrocarbonatites. Int. Geol. Rev. 36 (9), 797–819.
Lee, W., Wyllie, P.J., 1998a. Processes of crustal carbonatite formation by liquid immiscibility and differentiation, elucidated by model systems. J. Petrol. 39 (11), 2005–2013.
Lee, W.J., Wyllie, P.J., 1998b. Petrogenesis of carbonatite magmas from mantle to crust, constrained by the system CaO–(MgO + FeO*)–(Na_2O + K_2O)–(SiO_2 + Al_2O_3 + TiO_2)–CO_2. J. Petrol. 39 (3), 495–517.
Lee, W.J., Wyllie, P.J., 2000. The system CaO-MgO-SiO_2-CO_2 at 1 GPa, metasomatic wehrlites, and primary carbonatite magmas. Contrib. Miner. Petrol. 138 (3), 214–228.
Li, Z., Anenburg, M., Wei, C.-W., Yuan, N., Xu, C., 2024. Carbonatite metasomatism in a subvolcanic setting: Breccia at the Badou Carbonatite in the North China Craton and implications for magmatic evolution and eruptive style. J. Petrol. 65 (7), egae069.
Liu, Y., Anenburg, M., 2025. Reaction-driven magmatic crystallisation at the Maoniuping carbonatite. Nat. Commun. 16 (1), 7159.
Maki, I., Sugimura, T., 1970. Cubic metasilicate $Na_4CaSi_3O_9$ and its relation to tricalcium aluminate $Ca_3Al_2O_6$. J. Ceram. Assoc. Japan 78 (896), 129–132.
Martin, L.H.J., Schmidt, M.W., Mattsson, H.B., Guenther, D., 2013. Element partitioning between immiscible carbonatite and silicate melts for dry and H_2O-bearing systems at 1–3 GPa. J. Petrol. 54 (11), 2301–2338.
Massuyeau, M., Gardés, E., Morizet, Y., Gaillard, F., 2015. A model for the activity of silica along the carbonatite–kimberlite–mellilitite–basanite melt compositional joint. Chem. Geol. 418, 206–216.
Mitchell, R.H., 2005. Carbonatites and carbonatites and carbonatites. Can. Mineral. 43 (6), 2049–2068.
Mitchell, R.H., Gittins, J., 2022. Carbonatites and carbothermalites: a revised classification. Lithos 430–431, 106861.
Monecke, T., Kempe, U., Götze, J., 2002. Genetic significance of the trace element content in metamorphic and hydrothermal quartz: a reconnaissance study. Earth Planet. Sci. Lett. 202 (3–4), 709–724.
Moore, K.R., Brady, A.E., Costanzo, A., 2022. Crystal-liquid segregation in silicocarbonatite magma leads to the formation of calcite carbonatite. J. Petrol. 63 (7), egac056.
Mororó, E.A.A., Berkesi, M., Zajacz, Z., Guzmics, T., 2024. Rare earth element transport and mineralization linked to fluids from carbonatite systems. Geology 52 (4), 240–244.
Nabyl, Z., Gaillard, F., Tuduri, J., Carlo, I.D., 2021. No direct effect of F, Cl and P on REE partitioning between carbonate and alkaline silicate melts. Comptes Rendus. Géoscience 353 (S2), 233–272.
Nabyl, Z., Massuyeau, M., Gaillard, F., Tuduri, J., Iacono-Marziano, G., Rogerie, G., Le Trong, E., Di Carlo, I., Melleton, J., Bailly, L., 2020. A window in the course of alkaline magma differentiation conducive to immiscible REE-rich carbonatites. Geochim. Cosmochim. Acta 282, 297–323.
Otto, J.W., Wyllie, P.J., 1993. Relationships between silicate melts and carbonate-precipitating melts in CaO–MgO–SiO_2–CO_2–H_2O at 2 kbar. Mineral. Petrol. 48 (2–4), 343–365.
Paulsen, T., Deering, C., Sliwinski, J., Bachmann, O., Guillong, M., 2017. Evidence for a spike in mantle carbon outgassing during the Ediacaran period. Nat. Geosci. 10 (12), 930–934.
Pearce, M.L., 1964. Solubility of carbon dioxide and variation of oxygen ion activity in soda-silica melts. J. Am. Ceram. Soc. 47 (7), 342–347.
Ritchie, N.W., Newbury, D.E., Davis, J.M., 2012. EDS measurements of X-ray intensity at WDS precision and accuracy using a silicon drift detector. Microsc. Microanal. 18 (4), 892–904.
Ross, D.K., Simon, J.I., 2019. Evaluation of various methods for determining bulk compositions of chondrules and other objects in petrographic thin sections. Microsc. Microanal. 25 (S2), 2444–2445.
Ryabchikov, I.D., Kogarko, L.N., 2016. Deep differentiation of alkali ultramafic magmas: formation of carbonatite melts. Geochem. Int. 54 (9), 739–747.
Santoso, I., Riihimäki, M., Sibarani, D., Taskinen, P., Hupa, L., Paek, M.-K., Lindberg, D., 2022. Impact of recently discovered sodium calcium silicate solutions on the phase diagrams of relevance for glass-ceramics in the Na_2O-CaO-SiO_2 system. J. Eur. Ceram. Soc. 42 (5), 2449–2463.
Savard, J.J., Mitchell, R.H., 2021. Petrology of ijolite series rocks from the Prairie Lake (Canada) and Fen (Norway) alkaline rock-carbonatite complexes. Lithos 396–397, 106188.
Schmidt, M.W., Giuliani, A., Poli, S., 2024. The origin of carbonatites—Combining the rock record with available experimental constraints. J. Petrol. 65 (10), egae105.
Sharygin, V.V., Kamenetsky, V.S., Zaitsev, A.N., Kamenetsky, M.B., 2012. Silicate–natrocarbonatite liquid immiscibility in 1917 eruption combeite–wollastonite nephelinite, Oldoinyo Lengai Volcano, Tanzania: Melt inclusion study. Lithos 152, 23–39.
Stagno, V., Stopponi, V., Kono, Y., Manning, C.E., Irifune, T., 2018. Experimental determination of the viscosity of Na_2CO_3 melt between 1.7 and 4.6 GPa at 1200–1700 °C: Implications for the rheology of carbonatite magmas in the Earth's upper mantle. Chem. Geol. 501, 19–25.
Stone, R.L., 1954. Thermal analysis of magnesite at CO_2 pressures up to six atmospheres. J. Am. Ceram. Soc. 37 (2), 46–48.
Thompson, A.B., Aerts, M., Hack, A.C., 2007. Liquid immiscibility in silicate melts and related systems. Rev. Mineral. Geochem. 65 (1), 99–127.
Vasyukova, O., Kostyuk, A., Williams-Jones, A., 2023. Kovdor to Oldoinyo Lengai—The missing link in carbonatitic magma evolution. Geology 51 (1), 59–63.
Vasyukova, O.V., Williams-Jones, A.E., 2022. Carbonatite metasomatism, the key to unlocking the carbonatite-phoscorite-ultramafic rock paradox. Chem. Geol. 602, 120888.
Vasyukova, O.V., Williams-Jones, A.E., 2023. A new model for the origin of pyrochlore: evidence from the St Honoré Carbonatite, Canada. Chem. Geol. 632, 121549.
Veksler, I.V., Lentz, D., 2006. Parental magmas of plutonic carbonatites, carbonate–silicate immiscibility and decarbonation reactions: evidence from melt and fluid inclusions. In: Webster, J.D. (Ed.), Melt Inclusions in Plutonic Rocks. Mineralogical Association of Canada, Montreal, Quebec, pp. 123–149.
Veksler, I.V., Nielsen, T.F.D., Sokolov, S.V., 1998. Mineralogy of crystallized melt inclusions from Gardiner and Kovdor ultramafic alkaline complexes: implications for carbonatite genesis. J. Petrol. 39 (11–12), 2015–2031.
Voropaeva, D., Arzamastsev, A.A., Botcharnikov, R., Buhre, S., Gilbricht, S., Götze, J., Klemd, R., Schulz, B., Tichomirowa, M., 2024. LREE rich perovskite in antiskarn reactions - REE transfer from pyroxenites to carbonatites? Lithos 468–469, 107480.
Watkinson, D.H., Wyllie, P.J., 1971. Experimental study of the composition join $NaAlSiO_4$–$CaCO_3$–H_2O and the genesis of alkalic rock–carbonatite complexes. J. Petrol. 12 (2), 357–378.

Weidendorfer, D., Asimow, P.D., 2022. Experimental constraints on truly conjugate alkaline silicate – carbonatite melt pairs. Earth Planet. Sci. Lett. 584, 117500.
Weidendorfer, D., Schmidt, M.W., Mattsson, H.B., 2017. A common origin of carbonatite magmas. Geology 45 (6), 507–510.
Williams-Jones, A.E., Vasyukova, O.V., Kostyuk, A.V., 2024. Niobium ore genesis in a capsule. Geology 52 (7), 560–564.
Wyllie, P.J., Haas, J.L., 1965. The system $CaO–SiO_2–CO_2–H_2O$: 1. Melting relationships with excess vapor at 1 kilobar pressure. Geochim. Cosmochim. Acta 29 (8), 871–892.
Xiao, Y., Yang, W., Yang, X., Cao, Y., Tian, P., Zhao, Z., Hetherington, C., 2025. Mineralogical fingerprints of crustal silica contamination in the Bayan Obo carbonatite. Am. Mineral. 110 (3), 452–466.
Xue, S., Dasgupta, R., Ling, M.-X., Sun, W., Lee, C.-T.-A., 2024. The effect of fluorine on mineral-carbonatitic melt partitioning of trace elements – Implications for critical mineral deposits. Geochim. Cosmochim. Acta 379, 53–75.
Yang, D.-M., Hou, T., Botcharnikov, R.E., Veksler, I.V., Holtz, F., Zhang, Z., Zhang, L., Simon, A., Groschopf, N., 2024. An experimental study on the role of F^-, PO_4^{3-}, Cl^- and SO_4^{2-} ligands in the natrocarbonatite-nephelinite system at 850 °C and 0.1 GPa. Chem. Geol. 655, 122085.
Yaxley, G.M., Anenburg, M., Tappe, S., Decree, S., Guzmics, T., 2022. Carbonatites: classification, sources, evolution, and emplacement. Annu. Rev. Earth Planet. Sci. 50 (1), 261–293.
Yaxley, G.M., Kjarsgaard, B.A., Jaques, A.L., 2021. Evolution of carbonatite magmas in the upper mantle and crust. Elements 17 (5), 315–320.
Yuan, X., Yang, Z., Mayanovic, R.A., Hou, Z., 2024. Experimental evidence reveals the mobilization and mineralization processes of rare earth elements in carbonatites. Sci. Adv. 10 (27), eadm9118.
Yuan, X., Zhong, R., Xiong, X., Gao, J., Ma, Y., 2023. Transition from carbonatitic magmas to hydrothermal brines: continuous dilution or fluid exsolution? Sci. Adv. 9 (29), eadh0458.
Zech, R.F., Schmidt, M.W., Giuliani, A., 2025. Experimental differentiation of kimberlitic to carbonatitic melts: crystallization sequence and liquid line of descent. Contrib. Mineral. Petrol. 180 (12), 86.
Zhang, W., Chen, W.T., Zhang, X.-C., Tang, Y.-W., 2022. The trace element chemistry of quartz in carbonatite-related REE deposits: Implication for REE exploration. Ore Geol. Rev. 149, 105068.
Zheng, X., Liu, Y., Smith, M.P., Kynický, J., Hou, Z., 2023. Carbonatitic magma fractionation and contamination generate rare earth element enrichment and mineralization in the Maoniuping giant REE deposit, SW China. J. Petrol. 64 (6), egad037.